Comparison of Nested-Loop Rotors in Brushless Doubly-Fed Induction Machines

Wang, Xuezhou; Liu, Dong; Lahaye, Domenico; Polinder, Henk; Ferreira, Bram

Publication date
2017

Document Version
Accepted author manuscript

Published in
19th International Conference on Electrical Machines and Systems, ICEMS 2016

Comparison of Nested-Loop Rotors in Brushless Doubly-Fed Induction Machines

Xuezhou Wang*, Dong Liu*, Henk Polinder*, Domenico Lahaye** and Jan A. Ferreira*
*Department of Electrical Sustainable Energy, Delft University of Technology, Mekelweg 4, 2628 CD, Delft, the Netherlands
**Delft Institute of Applied Mathematics, Delft University of Technology, Mekelweg 4, 2628 CD, Delft, the Netherlands

***Abstract*—The brushless doubly-fed induction machine (DFIM) has great potential as a variable-speed generator for wind turbine applications. This special machine has a richer space-harmonic spectrum due to its special nested-loop rotor construction compared with conventional induction machines. It may result in higher iron losses, higher torque ripple and more time-harmonics adding to the grid total harmonic distortion (THD). This paper applies the 2D finite element (FE) model to investigate several different nested-loop rotor constructions. It shows the outer loop makes more contribution to the torque while the inner loop plays a small role in the torque production. The most outer loop determines the overall THD level while the inner one has little influence on it. The THD could be reduced by increasing the number of the outer loops. More machine performances could be studied to derive more guidelines for designing the middle loops.**

***Index Terms*—brushless, doubly-fed, induction machine, nested-loop rotor.**

I. Introduction

The brushless doubly-fed induction machine (DFIM) has gained a lot of research interest for wind turbine applications in recent years. It has the advantage of operating at variable speed with only a partially rated power converter just like a DFIM which is currently the most common generator for wind turbines [1]. Moreover, it has higher reliability because of the absence of brushes and slip rings. It also shows a better fault ride-through capability [2]. These benefits make the brushless DFIM a potential variable-speed wind generator, especially for off-shore installations.

Fig. 1 gives a typical structure of a brushless DFIM. The brushless DFIM has two stator AC windings with different pole-pairs and different frequencies. One of the stator windings is referred to as power winding (PW) and connected to the grid directly. The other one is called control winding (CW) and connected to the grid through a fractionally rated converter giving a variable frequency and voltage. There is no direct magnetic coupling between two stator windings. The magnetic coupling is achieved through a special rotor. More precisely, each stator winding is directly coupled to the rotor and 'cross-coupled' via the rotor to the other stator winding. Therefore, the rotor design is critical to the machine performance.

The research leading to these results has received funding from the European Union's Seventh Framework Programme managed by REA - Research Executive Agency (FP7/2007_2013) under Grant Agreement No.315485. The research leading to these results has received funding from the China Scholarship Council for supporting X. Wang's PhD research work.

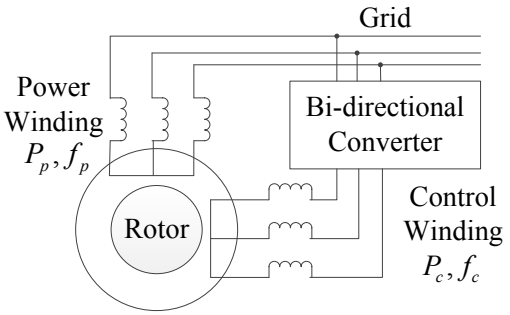

Fig. 1. The structure of brushless DFIM

There are generally three different kinds of rotors under investigation. They are reluctance rotors, wound rotors and cage rotors. Brushless doubly-fed reluctance machines (DFRMs) have slightly different operating principles. They are not in the scope of this paper. Wound rotors offer more flexible connections. A more complicated double-sine wound rotor is proposed for brushless DFIMs to reduce the space harmonics of the rotor winding [3]. It is designed to be constituted by double-layer unequal-turn coils based on the principles of tooth harmonic and sinusoidal winding. However, it is not straightforward to manufacture such complicated wound rotors. Compared with reluctance rotors and wound rotors, cages rotors have the advantages of ruggedness, lower impedance [4] and higher fill factors [5]. Moreover, it is cheaper to cast a cage rotor using aluminum or copper. However, special measures must be taken to achieve bar-to-stack insulation since the performance of brushless DFIMs is significantly degraded due to inter-bar currents [6]. The standard squirrel cage rotor gives a weak cross-coupling capability as can be expected. Among the rotors which show a strong cross-coupling capability, the nested-loop rotor construction is considered favorable because of its simplicity. Fig. 2 shows a typical construction of nested-loop rotors. This type of rotor comprises of nested loop terminated with a common end ring at one end only. The number of rotor nest should equal to $(p_p + p_c)$ to provide spatial compatibility for cross-coupling to happen [7].

Only a limited number of papers have studied the design of nested-loop rotors. Several different nested-loop rotors have been built and evaluated by measuring the torque-speed characteristics [8]. However, a higher average torque is not the only criterion for a better rotor design. Moreover, it is not straightforward to vary some configurations on a

Fig. 2. Nested-loop rotor constructions

prototype in the measurements. Equivalent circuit models (ECMs) have been applied to study the design of nested-loop rotors [9], [10]. The influence of the loop span and the number of loops per nest on the ECM parameters has been studied in [10]. However, the influence of different nested-loop rotors on torque ripples and harmonic distortions is not discussed. The rotor loops are proposed to be connect in series to improve the spatial distribution of the rotor magneto-motive force (MMF) [9]. This leads to a more complicated nested-loop rotor rather than giving a better design for the conventional nested-loop rotor shown in Fig. 2.

Finite element (FE) models have the advantages of taking into account saturation effects and detailed geometry constructions. They have been applied to study the influence of the number of loops per nest on the machine performance [11]. However, it is assumed that the rotor slots are distributed evenly along the rotor circumference. In fact, it has already shown that the most outer loop makes the biggest contribution to the average torque and the number of loops per nest has little influence on the average torque in the steady state [12].

The aim of this paper is to investigate the performance of different nested-loop rotor constructions using 2D transient FE models. The influence of the number of loops per nest and the position for each individual loop on the torque load-angle characteristics and total harmonic distortions will be compared. This paper starts with an introduction of the nested-loop rotor constructions studied. Next, the 2D transient FE models for brushless DFIMs are presented and the methods to calculate the electromagnetic torque and THD of induced voltages are given. Subsequently, the simulation results and discussions are illustrated to derive some design guidelines of nested-loop rotors. Finally, conclusions are drawn.

II. Rotor Constructions Studied

The stator construction is fixed to any rotor construction. Table I gives the main specifications of the brushless DFIM studied. Fig. 3 shows all the constructions studied in this paper. The construction a is the reference one. It has five loops per nest and rotor slots are distributed evenly along the rotor circumference. All the other constructions are developed from construction a. For ease of discussion, the most inner loop of construction a is signed as loop 1 and the most outer loop is sign as loop 5. To construction b, the loops from inner to outer are loop 2 to loop 5.

TABLE I
Main Specifications of the Studied BDFIM

Description	Machine parameter	Value
Axial length [mm]	L	240
Air-gap length [mm]	g	1
Stator outer radius [mm]	r_{so}	135
Stator inner radius [mm]	r_{si}	85
Rotor inner radius [mm]	r_{ri}	35
Number of phases	N_{ph}	3
Number of pole-pairs	p_p, p_c	2, 3
Rated frequency [Hz]	f_p, f_c	50, 10
Number of stator slots	N_{ss}	72
Number of rotor nests	p_r	5
Number of loops per nest	q_r	5, 4, 3
Rotor slot pitch in Fig. 3(a) [rad]		$\pi/25$

III. 2D Finite Element Model

A. Assumptions

To simplify the simulations, several assumptions are made in this paper:

1) The eddy current fields are neglected. This could be guaranteed since the eddy currents are reduced significantly due to the laminated structure in the iron core.
2) Skin effects and proximity effects are ignored for the stator windings and solid rotor bars.
3) The resistances of the end parts of the nested-loop rotors are taken into account in the coupled circuit equations, while the magnetic field produced by the end part is neglected.

B. Electromagnetic Field Equation

The above assumptions lead to a simplification that the electric conductivity σ is set as zero in all computing domains. The two-dimensional electromagnetic field equation is:

$$\frac{\partial}{\partial x}(\frac{1}{\mu}\frac{\partial A_z}{\partial x}) + \frac{\partial}{\partial y}(\frac{1}{\mu}\frac{\partial A_z}{\partial y}) = J_z(t). \tag{1}$$

where μ is the magnetic permeability of the material, A_z is the z component of the magnetic vector potential and J_z is the externally applied current density. In the air-gap and the iron core domains, J_z is zero. The stator current densities are given as:

$$J_{p(c)}(t) = \hat{J}_{p(c)} \sin(\omega_{p(c)} t + \phi_{p(c)}). \tag{2}$$

C. Coupled Circuit Equations

A field-circuit coupled model is applied to calculate the unknown rotor currents. Each loop of any nest could be considered as a short-circuited coil. Each closed loop has an independent circuit equation as:

$$e_r + i_r(R + X_\sigma) = 0, \tag{3}$$

where i_r is the induced rotor current of a certain loop, R is the resistance of that loop, X_σ is the leakage inductance

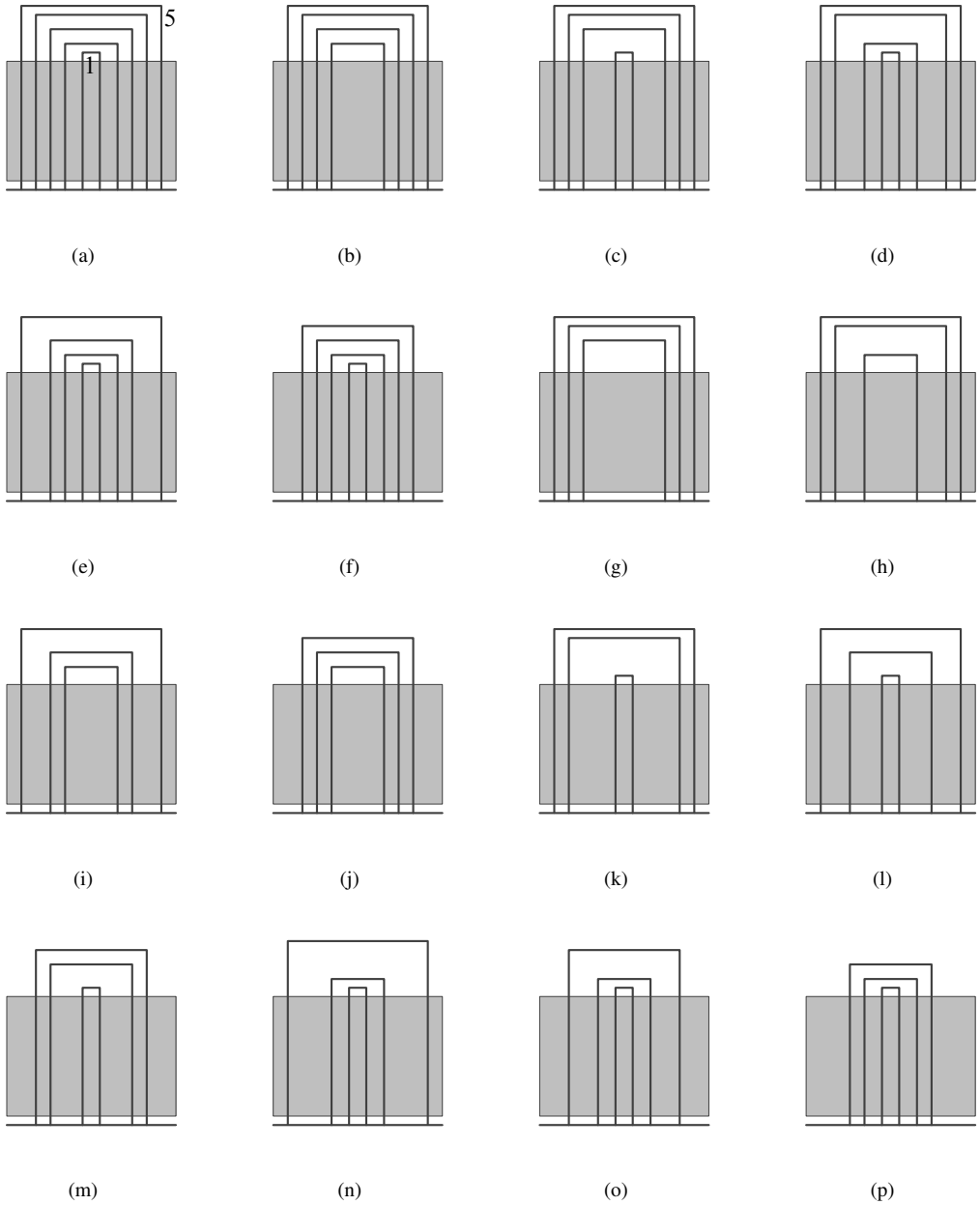

Fig. 3. Nested-loop rotor constructions

of the end part. e_r is the back electromotive force (EMF) of that loop, which can be calculated as [13]:

$$e_r(t) = -\frac{d\phi_r}{dt} = -\frac{L}{S}\frac{d(\iint A_z dS_+ - \iint A_z dS_-)}{dt}, \quad (4)$$

where ϕ_r is the flux linkage of a certain loop, L is the axial length of the machine, S is the cross-sectional area of the rotor bar, S_+ and S_- are the integration areas corresponding the go and return conductors, respectively. By substituting (4) into (3), the applied rotor current density of a certain loop is:

$$J_r(t) = \frac{L}{S^2(R + X_\sigma)}\frac{d(\iint A_z dS_+ - \iint A_z dS_-)}{dt}. \quad (5)$$

(5) relates the unknown rotor current densities with the total resultant magnetic field in which both stator and rotor currents are taken into account. The leakage inductance X_σ is not taken into account in this paper.

D. Post-processing

1) Electromagnetic torque: Maxwell's stress tensor method is applied to calculate the electromagnetic torque [14].

$$T = \frac{L}{\mu_0}\int_0^{2\pi} r^2 B_r B_t d\theta, \quad (6)$$

where μ_0 is the magnetic permeability of air, r is the radius of any contour circle in the air gap and θ is the angular position along the circumference of the contour circle, B_r

and B_t are the radial component and the tangential component of the air-gap flux density, respectively. The torque value slightly depends on the position of the contour circle if the meshes are not sufficiently fine. Therefore, rather than taking the line integration, the torque calculation could be more accurate by taking an integral over a band in the air-gap [14].

$$T = \frac{1}{\mu_0(r_1 - r_2)} \frac{r_1 + r_2}{2} \iint B_r B_t dS_g, \tag{7}$$

where r_1 and r_2 are the outer and inner radius of the air-gap band respectively and S_g is the cross sectional area of the band.

2) Total harmonic distortion (THD): The induced voltage of the power winding and the control winding can be calculated as:

$$e_{p(c)}(t) = -\frac{d\phi_{p(c)}}{dt}, \tag{8}$$

where $\phi_{p(c)}$ is the flux linkage of the power winding (or the control winding). It has a similar expression like ϕ_r given in (4). The influence of induced time harmonics in the induced power (or control) winding voltage can be evaluated by calculating the THD [15]:

$$THD_F = \frac{\sqrt{\sum_{h=2}^{\infty} E_{p(c),h}^2}}{E_{p(c),1}} \times 100\%, \tag{9}$$

where $E_{p(c),h}$ is the RMS voltage of the h^{th} harmonic and $h = 1$ is the fundamental frequency.

IV. Simulation Results and Discussions

A. Torque load-angle characteristics

A typical torque load-angle characteristics of the brushless DFIM is shown in Fig. 4. The brushless DFIM can operate like a synchronous machine. The load-angle is controlled by changing the phase angle between PW and CW currents. However, if the applied torque increases too much, the brushless DFIM cannot produce enough electromagnetic torque to operate in the stable range. It will then lose synchronism. Fig. 4 indicates the influences of the most outer loop on the torque load-angle characteristics. To rotor a and p, the most outer loops are loop 5 and loop 3, respectively. To rotor f, j, m, o, the most outer loops are loop 4. The most outer loop determines the average torque level. The brushless DFIM produces a bigger torque if the most outer loop of a nested-loop rotor has a bigger loop span. This is consistent with the conclusion of [10]. The extreme case with the biggest loop span is that the rotor has $(p_p + p_c)$ bars and several loops are located between adjacent bars. That rotor could be expected to produce a bigger average torque.

Fig. 5 gives the torque load-angle curves of rotors whose most outer loop is loop 5. Overall, they produce torques at the same level except the rotor n. Besides loop 5, rotor n contains loop 1 and 2. It means the inner loop makes less contribution to the torque. Fig. 5(b) gives the enlarge view of the curves. The torques produced in the sequence

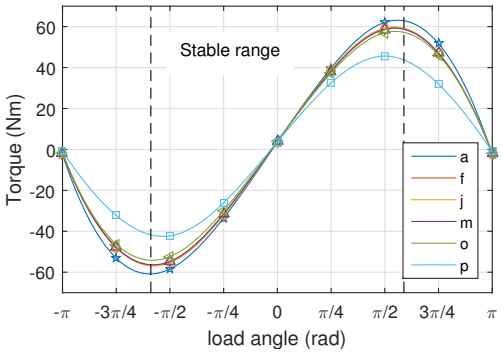

Fig. 4. Torque load-angle curves - influence of most outer loop

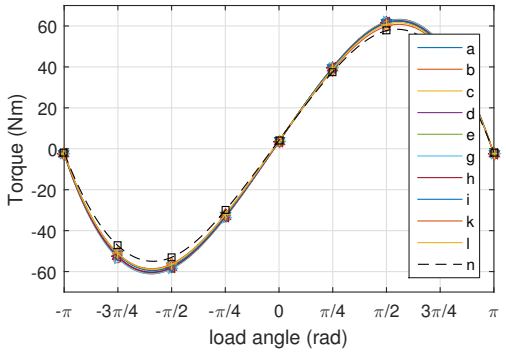

(a) All view

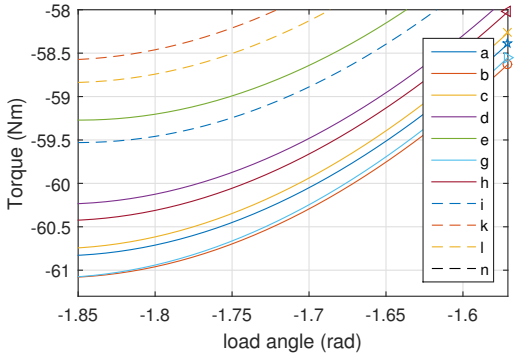

(b) Enlarge view

Fig. 5. Torque load-angle curves - rotors with loop 5

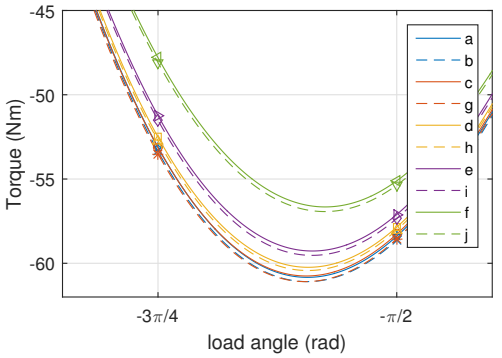

Fig. 6. Torque load-angle curves - influence of most inner loop

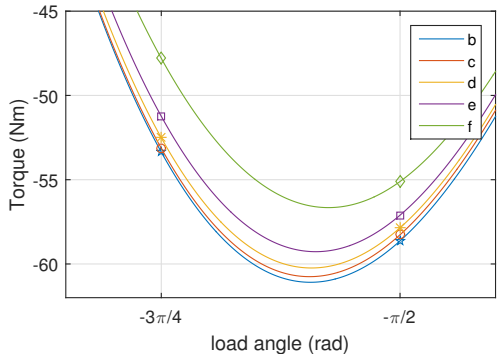

Fig. 7. Torque load-angle curves - influence of individual loop

from big to small are: $b > g > a > c > h > d > i > e > l > k > n$.

Fig. 6 indicates the influence of the most inner loop. The difference between a and b, c and g, d and h, e and i, f and j is the loop 1. The loop 1 makes a negative contribution to the torque. From the average torque point of view, it is better to leave out the most inner loop. It is loop 1 in this case study machine. However, it needs a further investigation to determine the exact loop span of the inner loop which could be left out.

Fig. 7 shows the torque load-angle curves of rotor b, c, d, e, f. It once again indicates that the importance of an individual loop exactly depends on its loop span.

B. Total harmonic distortion (THD)

Fig. 8 gives the THD of e_p and e_c. Similar to the torque load-angle curves, it shows that THDs have three levels with respect to different most outer loops. The rotor a with loop 5 leads to a lower THD than rotor p in which the most outer loop is loop 3. Rotor f, j, m, o, whose most outer loops are all loop 4, result in the THD at a similar level. It can be concluded that the loop span of the most outer loop could determine the overall THD level.

Fig. 9 shows the THD due to the rotors whose most outer loop is loop 5.They result in a similar THD level. Overall, rotor a, b lead to a relative lower THD level while rotor k, n lead to a higher THD level. Rotor g has the advantage of producing higher torques. However, it does not show the benefit on the THD. It can be conclude that more outer loops would result in a lower THD.

Fig. 10 shows the effects of loop 1. It is not straightforward to see whether it is a benefit to leaving out loop 1 for a lower THD. Fig. 11 gives the influence of an individual loop on the THD. Rotor f and e lead to a higher THD of e_p and e_c, respectively. Rotor c leads to a lower THD of e_p while rotor d leads to a lower THD of e_c.

V. Conclusion

This paper presents a comparison of nested-loop rotors. 2D transient FE models are applied to predict the torque load-angle characteristics and the THD of induced stator voltages. The loop span of the most outer loop should be

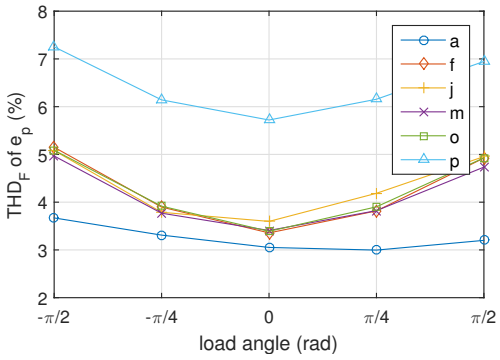

(a) THD_F of e_p

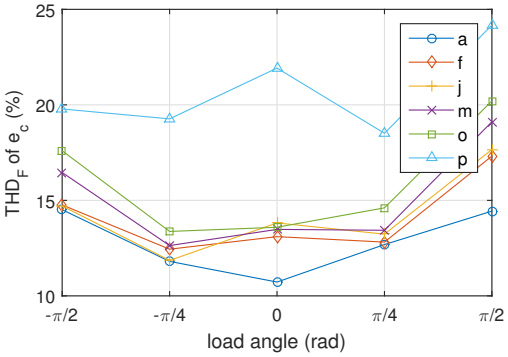

(b) THD_F of e_c

Fig. 8. Total harmonic distortion - influence of most outer loop

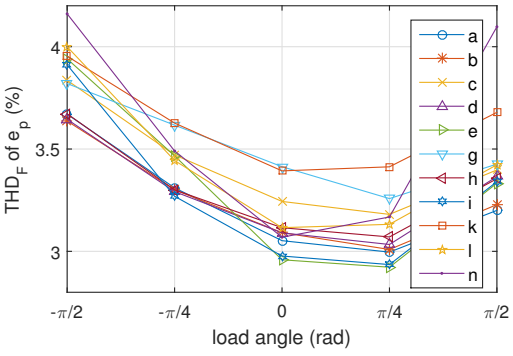

(a) THD_F of e_p

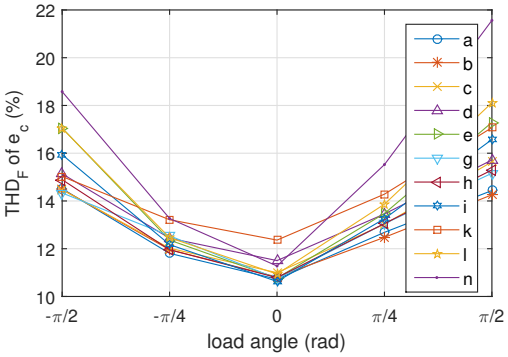

(b) THD_F of e_c

Fig. 9. Total harmonic distortion - rotors with loop 5

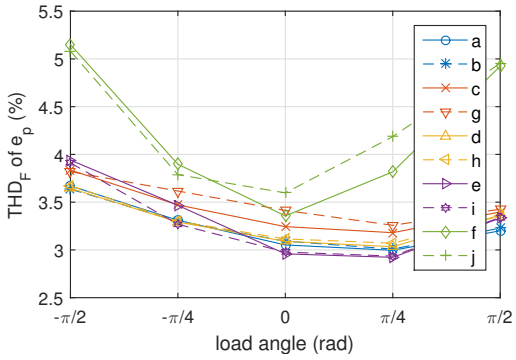

(a) THD_F of e_p

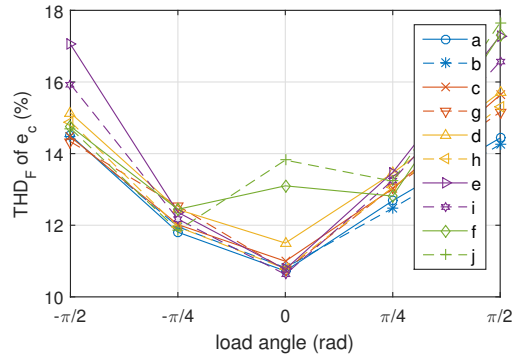

(b) THD_F of e_c

Fig. 10. Total harmonic distortion - influence of most inner loop

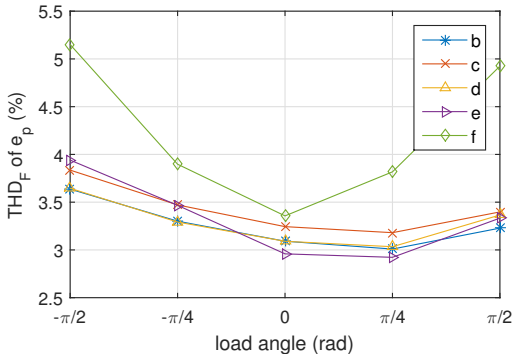

(a) THD_F of e_p

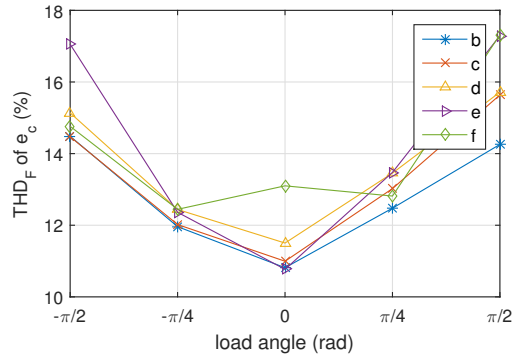

(b) THD_F of e_c

Fig. 11. Total harmonic distortion - influence of individual loop

as big as possible to achieve a bigger average torque and a lower THD of stator voltages. To the average torque, the contribution made by an individual loop exactly depends on its loop span. The inner loop with too small loop span could be left out for higher torque. However, the exact small loop span of the inner loop needs further investigations. To the THD, leaving out the most inner loop does not reduce the THD significantly. One possible way to reduce the THD is to increase the number of outer loops. However, the results of this paper do not indicate a clear influence of an individual loop locating in the middle on the THD. More aspects including torque ripple, core loss and efficiency could be studied to derive more guidelines for designing the middle loops.

REFERENCES

[1] H. Polinder, J. A. Ferreira, B. B. Jensen, A. B. Abrahamsen, K. Atallah, and R. A. McMahon, "Trends in wind turbine generator systems," *Emerging and Selected Topics in Power Electronics, IEEE Journal of*, vol. 1, no. 3, pp. 174–185, Sept. 2013.

[2] T. Long, S. Shao, E. Abdi, R. A. McMahon, and S. Liu, "Asymmetrical low-voltage ride through of brushless doubly fed induction generators for the wind power generation," *IEEE Transactions on Energy Conversion*, vol. 28, no. 3, pp. 502–511, 2013.

[3] X. Fei and W. Xuefan, "Design of a low-harmonic-content wound rotor for the brushless doubly fed generator," *Energy Conversion, IEEE Transactions on*, vol. 29, no. 1, pp. 158–168, Mar. 2014.

[4] X. Longya and W. Fengxiang, "Comparative study of magnetic coupling for a doubly fed brushless machine with reluctance and cage rotors," in *Industry Applications Conference, 1997. Thirty-Second IAS Annual Meeting, IAS '97., Conference Record of the 1997 IEEE*, vol. 1, Oct. 1997, pp. 326–332.

[5] R. McMahon, P. Tavner, E. Abdi, P. Malliband, and D. Barker, "Characterising brushless doubly fed machine rotors," *Electric Power Applications, IET*, vol. 7, no. 7, pp. 535–543, 2013.

[6] S. Williamson and M. S. Boger, "Impact of inter-bar currents on the performance of the brushless doubly fed motor," *IEEE Transactions on Industry Applications*, vol. 35, no. 2, pp. 453–460, Mar./Apr. 1999.

[7] T. D. Strous, X. Wang, H. Polinder, and J. A. Ferreira, "Brushless doubly-fed induction machines: magnetic field analysis," *Magnetics, IEEE Transactions on*, 2016.

[8] P. C. Roberts, "A study of brushless doubly-fed (induction) machines," Ph.D. dissertation, Cambridge University, 2005.

[9] H. Gorginpour, B. Jandaghi, and H. Oraee, "A novel rotor configuration for brushless doubly-fed induction generators," *IET Electric Power Applications*, vol. 7, no. 2, pp. 106–115, 2013.

[10] A. Oraee, E. Abdi, S. Abdi, R. McMahon, and P. J. Tavner, "Effects of rotor winding structure on the bdfm equivalent circuit parameters," *Energy Conversion, IEEE Transactions on*, vol. 30, no. 4, pp. 1660–1669, Dec. 2015.

[11] N. H. van der Blij, T. D. Strous, X. Wang, and H. Polinder, "A novel analytical approach and finite element modelling of a bdfim," in *Electrical Machines (ICEM), 2014 International Conference on*, Berlin, Germany, Sept. 2014, pp. 346–352.

[12] X. Wang, T. D. Strous, D. Lahaye, H. Polinder, and J. A. Ferreira, "Modeling and optimization of brushless doubly-fed induction machines using computationally efficient finite element analysis," *Industry Applications, IEEE Transactions on*, 2016.

[13] M. A. Jabbar, P. Hla Nu, and *et al.*, "Modeling and numerical simulation of a brushless permanent-magnet dc motor in dynamic conditions by time-stepping technique," *IEEE Transactions on Industry Applications*, vol. 40, no. 3, pp. 763–770, May/Jun. 2004.

[14] M. Popescu, "Prediction of the electromagnetic torque in synchronous machines through maxwell stress harmonic filter (hft) method," *Electrical Engineering*, 2006.

[15] S. Abdi, E. Abdi, A. Oraee, and R. McMahon, "Optimization of magnetic circuit for brushless doubly fed machines," *Energy Conversion, IEEE Transactions on*, vol. 30, no. 4, pp. 1611–1620, Dec. 2015.